

First evidence for off-shell Higgs boson production and the measurement of its width at CMS

Mostafa Mahdavihorrani^{1,2}

¹ Université Libre de Bruxelles and IIHE

² University of Antwerp

January 5, 2022

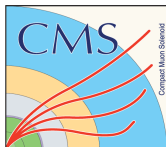


Table of contents

- 1 Phenomenology
- 2 Analysis strategy
- 3 Results
- 4 Summary

So far,

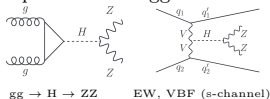
- 1964 \Rightarrow Brout-Englert-Higgs mechanism was introduced.
- 2012 \Rightarrow Discovered by ATLAS and CMS experiments with the pole mass $\simeq 125$ GeV.

Still we need to look for,

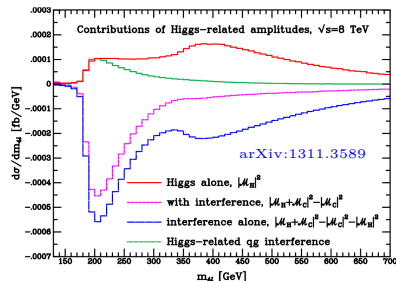
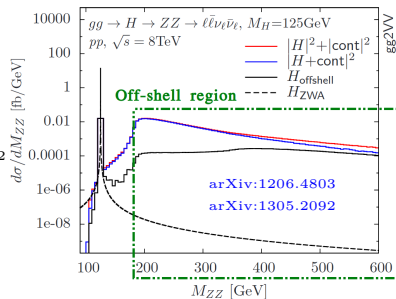
- Off-shell Higgs production \rightarrow sizable negative interference between Higgs ($\rightarrow VV$) and the continuum background \Leftarrow Unitarity
- Measurement for decay width (and thus life time) of Higgs boson. Resolution of direct measurement of the decay width is ~ 1 GeV \gg SM expectation of ~ 4.1 MeV
- BSM interactions in Higgs physics.

Off-shell Higgs production

- In SM, $H \rightarrow ZZ$ decay mode, more than 10% of the events are produced through off-shell production mode in the region with $m_{H^*} \geq 2m_Z$.
- when Higgs is off-shell, Higgs propagator square, $|D|^2 \propto 1/m_{ZZ}^4 \Rightarrow$ suppress the differential cross section
But when $\sqrt{q^2} \geq 2M_Z$ the decay part of Matrix element, $|\mathcal{M}_d(H \rightarrow ZZ)| \propto (m_{ZZ}^2)^2 \Rightarrow$ will cancel out the suppression from propagator
- The dominant processes are ggH and EW processes.



- Due to unitarity, in the SM there is a large and negative interference between signal and continuum VV production mode in the offshell region.



As pointed out in ref. [[arXiv:1307.4935](#)] for a process such as $i(\text{initial state}) \rightarrow H \rightarrow f(\text{final state})$, the differential cross section is:

$$\frac{d\sigma_{i \rightarrow H \rightarrow f}}{dM_f^2} \sim \frac{g_i^2 g_f^2}{(M_f^2 - m_H^2)^2 + m_H^2 \Gamma_H^2} \quad (1)$$

we can approximate the total cross section by integrating over on-shell region (a small region around m_H) and over very off-shell region ($M_f \gg m_H$),

$$\begin{aligned} \sigma_{i \rightarrow H \rightarrow f}^{\text{on-shell}} &\sim \frac{g_i^2 g_f^2}{m_H \Gamma_H} \\ \sigma_{i \rightarrow H^* \rightarrow f}^{\text{off-shell}} &\sim \frac{g_i^2 g_f^2}{M_f^2} \end{aligned}$$

Therefore the measurement of relative productions in both regions, provides us direct information on Γ_H

HVV interaction anomalous couplings

Anomalous couplings of HVV interactions may change the line-shape of m_{VV} and other kinematic variables and can be parametrized through HVV amplitude as in ref.

[arXiv:1307.4935,2002.09888,1610.07922],

$$A_{(HVV)} \sim \left[a_1^{VV} - e^{i\Phi_{\Lambda_1}} \frac{q_1^2 + q_2^2}{\Lambda_1^2} + \dots \right] m_V^2 \epsilon_{V1}^* \epsilon_{V2}^* \quad (3)$$

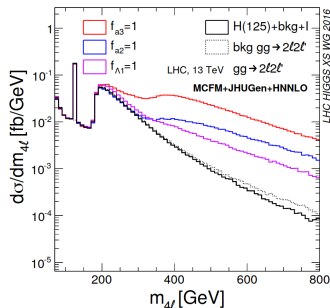
Dipole term

$$+ \underbrace{|a_2| e^{i\Phi_{a_2}} f_{\mu\nu}^{*(1)} f^{*(2),\mu\nu}}_{\text{CP-conserving}} - \underbrace{|a_3| e^{i\Phi_{a_3}} f_{\mu\nu}^{*(1)} \tilde{f}^{*(2),\mu\nu}}_{\text{CP-violating}}$$

- ϵ_i^μ and q_i^μ are polarization vector and 4-momentum of gauge boson V_i respectively.
- $f^{(i)\mu\nu} = \epsilon_i^\mu q_i^\nu - \epsilon_i^\nu q_i^\mu$, $\tilde{f}_{\mu\nu}^{(i)} = \frac{1}{2} \epsilon_{\mu\nu\rho\sigma} f^{(i)\rho\sigma} \rightarrow$ field and dual field strength tensors.
- a_1^{VV} are SM leading tree-level contributions in which only $a_1^{ZZ,WW} \neq 0$ and from custodial symmetry we have $a_1^{ZZ} = a_1^{WW}$.

We consider extreme scenarios of anomalous couplings a_2, a_3, Λ_1 , to constrain their strength $\tilde{f}_{ai} = f_{ai} \cos(\Phi_{ai})$ assuming $a_i \geq 0$, $\cos(\Phi_{ai}) = \pm 1$ where,

$$f_{ai} = \frac{|a_i|^2 \sigma_i}{\sum_j |a_j|^2 \sigma_j}, \quad a_j = a_1, a_2, a_3, \frac{1}{\Lambda_1^2} \quad (4)$$



- In this analysis we study the $2\ell 2\nu$ final state at high p_T^{miss} values and we consider off-shell Higgs production in $H \rightarrow ZZ \rightarrow 2\ell 2\nu$ as signal channel where $\ell = e, \mu$. The analysis is based on data collected by CMS experiment during LHC run 2 (2016-2018) at $\sqrt{s} = 13$ TeV and with integrated luminosity of $\sim 138\text{fb}^{-1}$.
- Since $2\ell 2\nu$ and 4ℓ final states have the same sensitivity in the off-shell region, we combine the results from off-shell $2\ell 2\nu$ with off-shell 4ℓ analysis [[arXiv:1901.00174](#)] to have a better precision on measurement of cross sections.
- For interpreting the results in terms of Γ_H and constraining anomalous couplings strength (\bar{f}_{ai}), the results from this analysis ($2\ell 2\nu$ final state) are combined with 4ℓ on-shell analyses from [[arXiv:1707.00541](#), [arXiv:2104.12152](#)].

CMS Physics Analysis Summary: HIG-21-013

Event selection and categorization

Events are categorized into 6 (3×2),

- $N_{\text{jet}} = 0$, $N_{\text{jet}} = 1$ and $N_{\text{jet}} \geq 2$
- $\mu\mu$ and ee

Event selections ("miss" = $p_{\text{T}}^{\text{miss}}$, $j = \text{jet with } p_{\text{T}} \geq 30 \text{ GeV}$ and $\ell = e, \mu$):

- Exactly 2 well-identified e/μ
 - $p_{\text{T}}^{\ell} \geq 25 \text{ GeV}$
 - $|\eta^{\ell}| < 2.4$ (for μ) and < 2.5 (for e)
- } leptons to be within acceptance

- $|m_{\ell\ell} - 91.2| < 15 \text{ GeV}$
 - $p_{\text{T}}^{\ell\ell} > 55 \text{ GeV}$
- } Requiring at least on on-shell high p_{T} Z boson

- No b-tagged jet
- } To reduce the background from $t\bar{t}$

- $p_{\text{T}}^{\text{miss}} > 125 \text{ GeV}$ if $N_j < 2$, else $> 140 \text{ GeV}$
 - $\Delta\phi_{\text{miss}}^{\ell\ell} > 1.0$
 - $\Delta\phi_{\text{miss}}^{\ell\ell+\text{jets}} > 2.5$
 - $\min \Delta\phi_{\text{miss}}^j > 0.25$ if $N_j = 1$, else > 0.5
- } To reduce the background from Drell-Yan

- Due to the $2\ell 2\nu$ final state in this analysis, we can not reconstruct the invariant mass of the ZZ system (m_{ZZ}), so instead we use ZZ system transverse mass m_T^{ZZ} defined as,

$$m_T^{ZZ2} = \left(\sqrt{p_T^{\ell\ell 2} + m_{\ell\ell}^2} + \sqrt{p_T^{\text{miss}2} + m_Z^2} \right)^2 - \left(\vec{p}_T^{\ell\ell} + \vec{p}_T^{\text{miss}} \right)^2 \quad (5)$$

- We use p_T^{miss} as the other observable since different backgrounds behave differently along p_T^{miss} , moreover, The shape of this variable is also sensitive to the presence of SM or BSM Higgs signal.
- In $N_j \geq 2$, matrix element likelihood ratio discriminants ($\mathcal{D}_{2\text{jet}}^{\text{VBF}, a_i}$) are used to discriminate VBF production mechanism from ggH:

$$\mathcal{D}_{2\text{jet}}^{\text{VBF}, a_i} = \frac{\mathcal{P}_{\text{VBF}}^{a_i}}{\mathcal{P}_{\text{VBF}}^{a_i} + \mathcal{P}_{\text{QCD H}+2\text{jet}}^{\text{SM}}} \quad (6)$$

where \mathcal{P} is the matrix element probability density computed by MELA package [[Github](#)] using four momenta of

- the two leading- p_T jets
- Higgs boson by utilizing $\eta_{\nu\nu} = \eta_{\ell\ell}$ approximation.

Signal and interfering background modeling

Signal, interfering backgrounds and interference components for SM/BSM hypotheses are obtained using simulation samples at NLO QCD and reweighting techniques:

- 1) Using samples with different Higgs pole mass (from 125 GeV to 3 TeV) produced via POWHEG NLO QCD for Higgs production and JHUGen for Higgs decay.
- 2) Reweighting POWHEG/JHUGen samples by ratio of matrix element probability densities computed by MELA package by approximating LO topology from NLO topology.
- 3) Stitching the reweighted samples to obtain final distributions.

Corrections on ggH production mode

- NNLO k-factor(m_{VV}) $\times 1.1$ flat N3LO QCD corrections are applied.
- The same corrections are applied on all interfering components with additional 10% uncertainty applied to the continuum gg \rightarrow ZZ production component

- $q\bar{q} \rightarrow ZZ, WZ$ are the dominant backgrounds at high m_T^{ZZ}
 - Estimated from simulation
 - EW correction at NLO are applied as k-factors
 - Joint fit with 3ℓ WZ control region (CR) to improve the estimation.
- Events in Drell-Yan process with high fake p_T^{miss} coming from instrumental sources (instrumental p_T^{miss})
 - Can not be well estimated from simulation
 - Estimated from data-driven method in single-photon CR
 - Real p_T^{miss} contained processes ($Z\gamma, W\gamma, W+\text{jets}$) in this CR are estimated and subtracted from the reweighted data
- Nonresonant backgrounds (top, WW, W+jets processes)
 - Estimation from simulation is not optimal in our phase space
 - Estimated from data-driven method in $e\mu$ CR
 - Events are reweighted for lepton ID/isolation and trigger efficiencies,
- Minor contributions from e.g. $tZ + X$ processes are fully estimated from simulation

Most of the systematics affect both the shape and normalization

- Theoretical uncertainties:

- Renormalization scale and Factorization scale (up to 30%)
- $\alpha_S(m_Z)$ and PDF variations (up to 20%)
- Simulation of the second jet in gg samples (up to 20%)
- Scale and tune variations of PYTHIA
- NLO EW correction ($q\bar{q} \rightarrow ZZ, WZ$)
- Uncorrelated uncertainties on $N_j = 0$ (2.7%), $N_j = 1$ (6.0%) and $N_j \geq 2$ (7.6%) in $q\bar{q} \rightarrow ZZ, WZ$ derived from the 3ℓ CR

- Instrumental uncertainties on simulations:

- Luminosity (between 1.2% and 2.5%, depending on the data taking period)
- L1 prefire scale
- Pile-up, JES, JER and p_T^{miss} resolution correction
- Uncertainties in lepton, trigger, pile-up jet identification, and b-tagging efficiencies (typically 1% per lepton)

Statistical uncertainties on simulations are also taken into account.

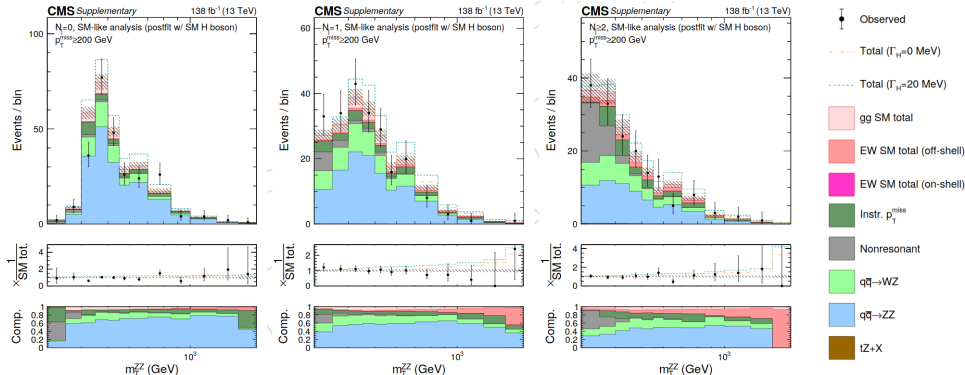


Figure 2: Shows the postfit distributions of m_T^{ZZ} in the $N_j = 0$ (left), $= 1$ (middle), and ≥ 2 (right) categories $2\ell 2\nu$ signal region. Postfit refers to a combined $2\ell 2\nu + 4\ell$ fit assuming SM H boson parameters. The middle pads on the bottom panels show the ratio of the data or dashed histograms to the stacked histogram, and the bottom pads show the relative contributions of each process in the stacked histogram

Summary distributions

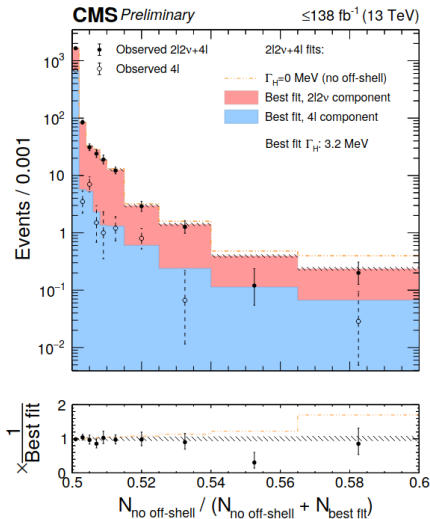
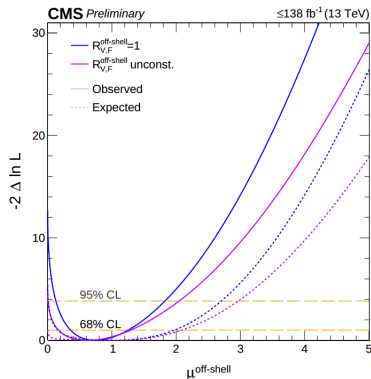
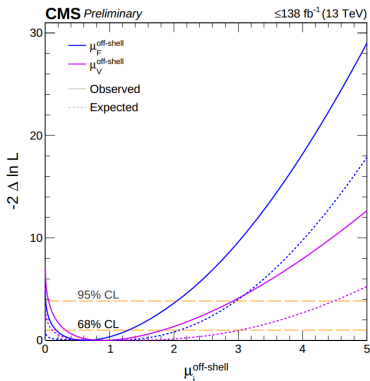


Figure 4: Distributions of postfit ratios of the number of events in each $2l2\nu$ and 4ℓ off-shell signal region bin. The ratios are taken after separate fits to the $\Gamma_H = 0 \text{ MeV}$ hypothesis and the best overall fit. The stacked histograms display the contributions after the best fit, and the gold dashed line shows the distribution of these ratios for a fit to the $\Gamma_H = 0 \text{ MeV}$ hypothesis.

Results on off-shell signal strength parameters



Presence of Higgs off-shell production can be quantified by measuring the signal strength parameters ($\mu = \sigma^{\text{obs}}/\sigma^{\text{SM}}$) such as $\mu_F^{\text{off-shell}}$ for ggH and $\mu_V^{\text{off-shell}}$ for EW, or a common $\mu^{\text{off-shell}}$ width different conditions on $R_{V,F}^{\text{off-shell}} = \mu_V^{\text{off-shell}}/\mu_F^{\text{off-shell}}$ to be = 1 or unconstrained.

$\mu^{\text{off-shell}} = 0$ ($R_{V,F}^{\text{off-shell}} = 1$) is excluded with more than 99.9% C.L (3.6 standard deviations)

Param.	Cond.	Observed	Expected
$\mu_F^{\text{off.}}$	$\mu_V^{\text{off.}}$ (u)	$0.62^{+0.68}_{-0.45}$	$1^{+1.1}_{-0.99998}$
$\mu_V^{\text{off.}}$	$\mu_F^{\text{off.}}$ (u)	$0.90^{+0.9}_{-0.59}$	$1^{+2.0}_{-0.89}$

Table 2: Summary of results on the signal strength and Γ_H . Results for Γ_H (in units of) are obtained with the signal strengths unconstrained. Tests with anomalous HVV couplings are distinguished by the denoted cross section fractions.

Param.	Cond.	Observed	Expected
Γ_H	SM-like	$3.2^{+2.4}_{-1.7}$	$4.1^{+4.0}_{-3.5}$
Γ_H	f_{a2} (u)	$3.4^{+2.3}_{-1.8}$	$4.1^{+3.9}_{-3.6}$
Γ_H	f_{a3} (u)	$2.7^{+2.1}_{-1.4}$	$4.1^{+3.9}_{-3.6}$
Γ_H	$f_{\Lambda 1}$ (u)	$2.7^{+2.1}_{-1.4}$	$4.1^{+4.0}_{-3.6}$

Results interpretations on BSM HVV couplings

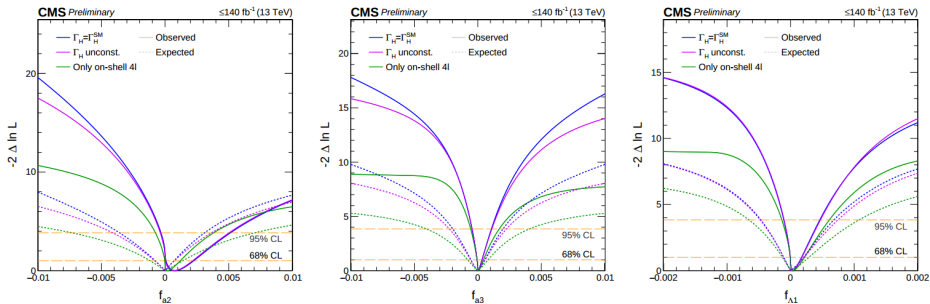


Figure 6: Shows the likelihood scans of f_{a_2} (left), f_{a_3} (middle), and $f_{\Lambda 1}$ (right) are shown with the constraint $\Gamma_H = \Gamma_H^{\text{SM}}$ (blue), Γ_H unconstrained (violet), or based on on-shell 4ℓ only (green). Observed (expected) scans are shown with solid (dashed) curves. The horizontal lines indicate the 68% and 95% CL regions.

VBF/VBS candidate from the $N_j \geq 2$ category in the $2\ell 2\nu$ SR

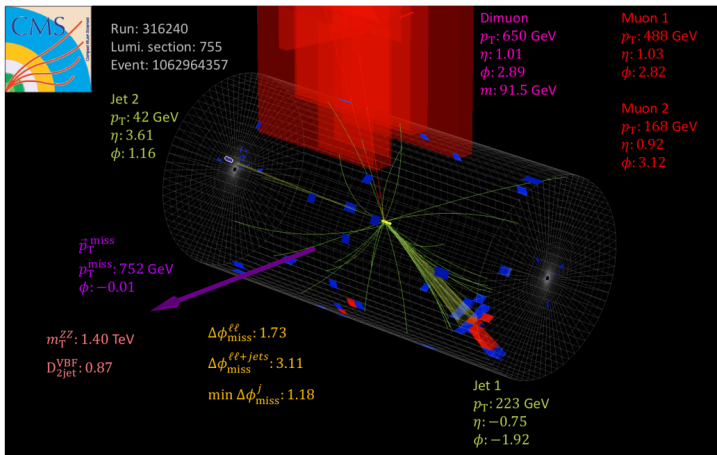


Figure 1 : Shown is a VBF/VBS candidate from the $N_j \geq 2$ category in the $2\ell 2\nu$ signal region. The two jets pointed at opposite hemispheres, the high p_T^{miss} value, and the central, high- p_T dilepton system make this event one of the ideal candidates for this topology, as also evident by the high $D_{2\text{jet}}^{\text{VBF}} = 0.87$ value computed for this event.

- The CMS $2\ell 2\nu$ offshell analysis of 2016-2018 proton-proton collision data at $\sqrt{s} = 13$ TeV was completed and shows good sensitivity to offshell ($m_{VV} > 2m_V$) H production.
- The combination of $2\ell 2\nu$ off-shell analysis with published 4ℓ analyses resulted in finding an evidence for the first time for off-shell Higgs production and Γ_H is measured ($\Gamma_H = 3.2^{+2.4}_{-1.7}$ MeV) based on this evidence.
- Constraints on anomalous couplings shows no significant deviation from SM.
- The CMS Physics Analysis Summary of this analysis (HIG-21-013) can be found [\[here\]](#)
- CMS Physics briefing of the analysis can be found [\[here\]](#)
- We are aiming to publish the results in Nature Physics journal.

Backup

Table 2: Comparisons between the number of observed events in the $2\ell 2\nu$ channel with expectations from the SM and no-off-shell scenarios as a function of N_j for low and high m_{T}^{ZZ} . An additional requirement of $p_{\text{T}}^{\text{miss}} \geq 200$ GeV has been imposed for $N_j \geq 2$.

	m_{T}^{ZZ}	$N_j = 0$	$N_j = 1$	$N_j \geq 2$
SM	< 450 GeV	1118_{-49}^{+45}	660_{-40}^{+31}	92_{-8}^{+7}
No off.	< 450 GeV	1127_{-49}^{+46}	666_{-40}^{+31}	93_{-8}^{+7}
Data	< 450 GeV	989	643	95
SM	≥ 450 GeV	241_{-14}^{+13}	166_{-12}^{+10}	68_{-6}^{+5}
No off.	≥ 450 GeV	252_{-14}^{+14}	178_{-13}^{+10}	75_{-6}^{+5}
Data	≥ 450 GeV	217	151	66

Sensitivity of off-shell $2\ell 2\nu$ channel, CMS

Table 4: Constraints on the $\mu_F^{\text{off-shell}}$, $\mu_V^{\text{off-shell}}$, and $\mu^{\text{off-shell}}$ parameters are summarized. The constraints on $\mu^{\text{off-shell}}$ are obtained with $R_{V,F}^{\text{off-shell}}$ unconstrained or = 1. The measurements are presented using the $2\ell 2\nu$ analysis alone, or with the inclusion of off-shell 4ℓ events. The designation ‘c.v.’ stands for the central value obtained in the likelihood scan, and the expected central value is always unity, so it is not quoted explicitly.

Parameter	Condition	c.v.	Observed		Expected	
			68% 95% CL	68% 95% CL		
$\mu_F^{\text{off-shell}}$ ($2\ell 2\nu + 4\ell$)	$\mu_V^{\text{off-shell}}$ unconst.	0.62	[0.17, 1.3] [0.0060, 2.0]	$[2 \cdot 10^{-5}, 2.1]$ < 3.0		
$\mu_F^{\text{off-shell}}$ ($2\ell 2\nu$)	$\mu_V^{\text{off-shell}}$ unconst.	0.41	[0.014, 1.4] < 2.6	< 2.5 < 3.7		
$\mu_V^{\text{off-shell}}$ ($2\ell 2\nu + 4\ell$)	$\mu_F^{\text{off-shell}}$ unconst.	0.90	[0.31, 1.8] [0.051, 2.9]	$[0.11, 3.0]$ < 4.5		
$\mu_V^{\text{off-shell}}$ ($2\ell 2\nu$)	$\mu_F^{\text{off-shell}}$ unconst.	1.1	[0.28, 2.4] [0.016, 3.8]	$[0.07, 3.2]$ < 4.8		
$\mu^{\text{off-shell}}$ ($2\ell 2\nu + 4\ell$)	$R_{V,F}^{\text{off-shell}} = 1$	0.74	[0.36, 1.3] [0.13, 1.8]	$[0.16, 2.0]$ $[0.0086, 2.7]$		
$\mu^{\text{off-shell}}$ ($2\ell 2\nu + 4\ell$)	$R_{V,F}^{\text{off-shell}}$ unconst.	0.62	[0.17, 1.3] [0.0061, 2.0]	$[4 \cdot 10^{-5}, 2.1]$ $[1 \cdot 10^{-5}, 3.0]$		
$\mu^{\text{off-shell}}$ ($2\ell 2\nu$)	$R_{V,F}^{\text{off-shell}} = 1$	0.74	[0.25, 1.5] [0.043, 2.3]	$[0.11, 2.3]$ $[2 \cdot 10^{-4}, 3.2]$		
$\mu^{\text{off-shell}}$ ($2\ell 2\nu$)	$R_{V,F}^{\text{off-shell}}$ unconst.	0.41	[0.014, 1.4] $[2 \cdot 10^{-5}, 2.6]$	$[3 \cdot 10^{-5}, 2.5]$ $[6 \cdot 10^{-6}, 3.7]$		

Table 10: Summary of allowed 68% CL (central values with uncertainties) and 95% CL (in square brackets) intervals for $\mu^{\text{off-shell}}$, $\mu_{\text{F}}^{\text{off-shell}}$, and $\mu_{\text{V}}^{\text{off-shell}}$ obtained from the analysis of the combination of Run 1 and Run 2 off-shell data sets.

Parameter	Observed	Expected
$\mu^{\text{off-shell}}$	$0.78^{+0.72}_{-0.53}$ [0.02, 2.28]	$1.00^{+1.20}_{-0.99}$ [0.0, 3.2]
$\mu_{\text{F}}^{\text{off-shell}}$	$0.86^{+0.92}_{-0.68}$ [0.0, 2.7]	$1.0^{+1.3}_{-1.0}$ [0.0, 3.5]
$\mu_{\text{V}}^{\text{off-shell}}$	$0.67^{+1.26}_{-0.61}$ [0.0, 3.6]	$1.0^{+3.8}_{-1.0}$ [0.0, 8.4]

[arXiv:1901.00174](https://arxiv.org/abs/1901.00174)

Table 2: The 95% CL upper limits on $\mu_{\text{off-shell}}$, $\Gamma_H/\Gamma_H^{\text{SM}}$ and R_{gg} . Both the observed and expected limits are given. The 1σ (2σ) uncertainties represent 68% (95%) confidence intervals for the expected limit. The upper limits are evaluated using the CL_s method, with the SM values as the alternative hypothesis for each interpretation.

		Observed	Median	Expected	
				$\pm 1 \sigma$	$\pm 2 \sigma$
$\mu_{\text{off-shell}}$	$ZZ \rightarrow 4\ell$ analysis	4.5	4.3	[3.3, 5.4]	[2.7, 7.1]
	$ZZ \rightarrow 2\ell 2\nu$ analysis	5.3	4.4	[3.4, 5.5]	[2.8, 7.0]
	Combined	3.8	3.4	[2.7, 4.2]	[2.3, 5.3]
$\Gamma_H/\Gamma_H^{\text{SM}}$	Combined	3.5	3.7	[2.9, 4.8]	[2.4, 6.5]
R_{gg}	Combined	4.3	4.1	[3.3, 5.6]	[2.7, 8.2]

[arXiv:1808.01191v2](https://arxiv.org/abs/1808.01191v2)

Results on off-shell signal strength parameters

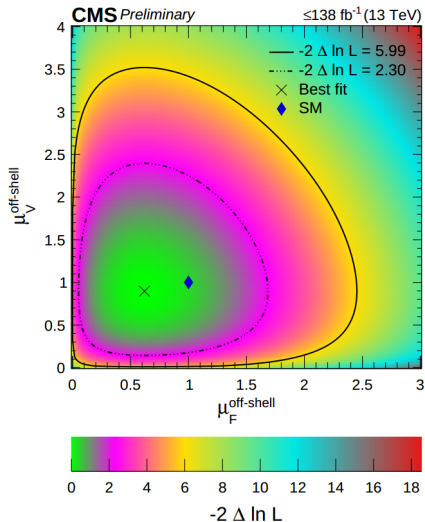


Figure 4: Shows the two-parameter likelihood scan of $\mu_F^{\text{off-shell}}$ and $\mu_V^{\text{off-shell}}$. The dot-dashed and solid contours enclose the 68% and 95% CL regions. The cross marks the minimum, and the blue rhombus mark is the SM expectation

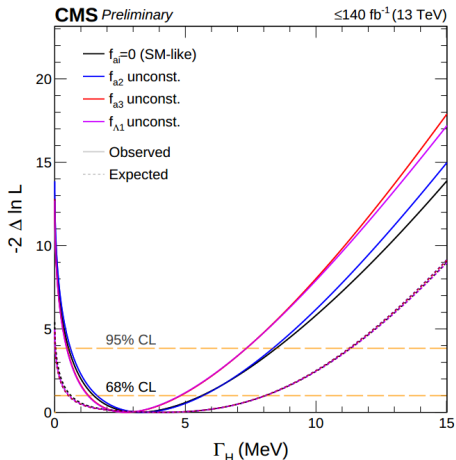


Figure 5: The likelihood scan of Γ_H with different constraints on Γ_H are shown with and without anomalous HVV couplings. The horizontal lines indicate the 68% and 95% CL regions.

The width of the H boson is observed to be $\Gamma_H = 3.2$ MeV and is constrained within the interval [1.5, 5.6] and [0.62, 8.1] at 68% confidence for observed and expected respectively.